DMD Fast Forward. Published on October 11, 2017 as DOI: 10.1124/dmd.117.077818
This article has not been copyedited and formatted. The final version may differ from this version.

Title Page

Metabolic epoxidation is a critical step for the development of benzbromarone-induced hepatotoxicity

Hui Wang, Ying Peng, Tingjian Zhang, Qunsheng Lan, Huimin Zhao, Wenbao Wang, Yufei Zhao, Xu Wang, Jianxin Pang, Shaojie Wang, Jiang Zheng

Wuya College of Innovation (H. W., Y. P., H. Z., Y. Z., X. W., J. Z.), Shenyang Pharmaceutical University, Shenyang, Liaoning, 11016, P. R. China; School of Pharmacy (T. Z.), China Medical University, Shenyang, Liaoning, 110122, P. R. China; Guangdong Provincial Key Laboratory of Drug Screening (Q. L., J. P.), School of Pharmaceutical Sciences, Southern Medical University, Guangzhou, Guangdong, 510515, P. R. China; Key Laboratory of Structure-Based Drug Design & Discovery (Ministry of Education) (W. W., S. W.), School of Pharmaceutical Engineering, Shenyang Pharmaceutical University, Shenyang, 110016, P. R. China; State Key Laboratory of Functions and Applications of Medicinal Plants (J. Z.), Key Laboratory of Pharmaceutics of Guizhou Province (J. Z.), Guizhou Medical University, Guiyang, Guizhou, 550004, P. R. China.

DMD Fast Forward. Published on October 11, 2017 as DOI: 10.1124/dmd.117.077818
This article has not been copyedited and formatted. The final version may differ from this version.

Running Title Page

Running title: Epoxidation and hepatotoxicity of benzbromarone

Corresponding Authors:

Jianxin Pang
School of Pharmaceutical Sciences, Southern Medical University, 1838 North Guangzhou Ave, Guangzhou, Guangdong, 510515, China.

E-mail: pjx@smu.edu.cn
Tel: +86-20-61648671
Fax: +86-20-61648671

Shaojie Wang
School of Pharmaceutical Engineering, Shenyang Pharmaceutical University, 103 Wenhua Rode, Shenyang, Liaoning, 110016, P. R. China.

E-mail: sjwang_99@163.com
Tel: +86-24-43520230
Fax: +86-24-43520230

Jiang Zheng
Wuya College of Innovation, Shenyang Pharmaceutical University, 103 Wenhua Rode, Shenyang, Liaoning, 110016, P. R. China; State Key Laboratory of Functions and Applications of Medicinal Plants, Key Laboratory of Pharmaceutics of Guizhou Province, Guizhou Medical University, Guiyang, Guizhou, 550004, P. R. China.

E-mail: zhengneu@yahoo.com
Tel: +86-24-23986361
Fax: +86-24-23986510

The number of text pages: 30
The number of tables: 3
The number of figures: 10
The number of schemes: 1
The number of references: 43
The number of words in the *Abstract*: 194
The number of words in the *Introduction*: 637
The number of words in the *Discussion*: 1389

Abbreviations

ALT, alanine transaminase; AST, aspartate transaminase; BBR, benzbromarone; CE, collision energy; CL_{int}, intrinsic clearance; CUR, curtain gas; CXP, cell exit potential; DMEM, Dulbecco's modified Eagle's medium; DP, declustering potential; DPBS, dulbecco's phosphate buffered saline; ESI, electrospray ionization; GS1, ion source gas 1; GS2, ion source gas 2; GSH, glutathione; hURAT1, human urate transporter 1; HLMs, human liver microsomes; HRESIMS, high resolution electrospray ionization mass spectroscopy; LC-MS/MS, liquid chromatography coupled to tandem mass spectrometry; mBrB, monobromobimane; MDCK, Madin-Darby Canine Kidney; MLMs, mouse liver microsomes; MRM, multiple-reaction monitoring; NAC, *N*-acetylcysteine; NADPH, *β*-nicotinamide adenine dinucleotide 2′-phosphate reduced tetrasodium salt; P450, cytochrome P450; PO, potassium oxonate; RLMs, rat liver microsomes; SUA, serum uric acid; $t_{1/2}$, half-life; TLC, thin-layer chromatography.

Abstract

Benzbromarone (BBR) is effective in the treatment of gout but can also cause fatal hepatic failure in clinic. Our early studies demonstrated that CYP3A catalyzed the biotransformation of BBR to epoxide intermediate(s) which reacted with sulfur nucleophiles of protein to form protein covalent binding both *in vitro* and *in vivo*. The present study attempted to define the correlation between metabolic epoxidation and hepatotoxicity of BBR by manipulating the structure of BBR. We rationally designed and synthesized three halogenated BBR derivatives (6-F-, Cl-, or Br-BBR) to decrease the potential for P450-mediated metabolic activation. Both *in vitro* and *in vivo* uricosuric activity assays showed that the fluorinated BBR (6-F-BBR) achieved favorable uricosuric effect, while the chlorinated BBR (6-Cl-BBR**)** and brominated BBR (6-Br-BBR) showed weak uricosuric efficacy. Additionally, 6-F-BBR elicited much lower hepatotoxicity in mice. Fluorination of BBR offered advantage to metabolic stability in liver microsomes, almost completely blocked the formation of epoxide metabolite(s) and protein covalent binding, and attenuated hepatic and plasma GSH depletion. Moreover, the structural manipulation did not alter the efficacy of BBR. This work provided solid evidence that the formation of the epoxide(s) is a key step for the development of BBR-induced hepatotoxicity.

Introduction

Gout is the most prevalent inflammatory arthritis and occurs in approximately 0.2% to 0.35% of the general population (Fernandes et al., 2017). Specifically, gout is an inflammatory arthritis characterized by deposition of urate in articular cartilage or periarticular tissues (Perez-Ruiz et al., 2015; Keenan and Schlesinger, 2016). Overproduction of uric acid and deficiency in renal excretion contribute to elevated serum urate which is known as hyperuricemia. The incidence of gout grows is considered to partially result from the decline of renal function (Smith et al., 2010). Genetic and dietary factors also influence uric blood levels (Doherty, 2009). Recent studies suggest that hyperuricemia plays essential roles in some important diseases such as cardiovascular disease, diabetes, hypertension, and chronic renal disease (Baker and Schumacher, 2010; Ruoff and Edwards, 2016). Gout has been a threat to human health, and the needs for effective drugs that lower serum urate levels are therapeutically urgent.

Insufficient renal excretion was reported to account for 70% of urate load (Choi et al., 2005; Abhishek et al., 2017). Consequently, uricosurics that act directly on the renal tubule and increase urate renal excretion by inhibiting uric acid reabsorption emerge. Among commercially available uricosurics, benzbromarone (BBR, Figure 1) is extremely potent and well tolerated, with most people meeting treatment goals, compared with probenecid and sulfinpyrazone (Abhishek et al., 2016). As a uricusuric, BBR shows potent inhibition property to human urate transporter 1 (hURAT1), a known transporter responsible for urate reabsorption (Wempe et al., 2011; Ahn et al., 2016). Though effective, BBR is not licensed for use in the United

States, due to several reported idiosyncratic hepatotoxic events (Arai et al., 2002; Lee et al., 2008; Kydd et al., 2014).

It is widely accepted that cytochromes P450 (P450)-mediated metabolic activation is most frequently responsible for drug induced idiosyncratic hepatotoxicity and drug withdrawal from the market (Leung et al., 2012; Dekker et al., 2016; Xuan et al., 2016). Our early metabolic studies illustrated that CYP3A metabolized BBR to epoxide intermediate(s) which reacted with sulfur nucleophiles of protein to form protein covalent binding both *in vitro* and *in vivo* (Wang et al., 2016a; Wang et al., 2016b). In an attempt to define the association between BBR bioactivation and its hepatotoxicity, we modified the structure of BBR by decreasing the potential for the P450-mediated metabolic activation and then evaluated the toxicological and pharmacological responses to the structural manipulation.

Incorporation of halogens in drugs is a commonly employed strategy when decrease in P450 metabolic degradation is needed (Wilcken et al., 2013; Ford and Ho, 2016; Obach et al., 2016). In the lead optimization of Ezetimib, a cholesterol inhibitor, benzylic oxidation was blocked by introduction of fluorine at the phenyl ring to mitigate P450-mediated oxidation (Rosenblum et al., 1998; Purser et al., 2008). Bromination or iodination proximal to the phenolic hydroxyl group was carried out in structural optimization of 13α-estrone to prevent the generation of reactive quinone intermediates that might participate in estrogen-induced carcinogenesis (Patel and Bhat, 2004; Bacsa et al., 2015). It is convinced that by inserting halogens adjacent to or substitution of metabolically labile sites, the potential for metabolic clearance can

be attenuated by lowing metabolic rate or blocking metabolic pathways. Besides, halogen substituents are frequently utilized to improve membrane permeability and, therefore, to enhance oral absorption (Lu et al., 2010; Ford and Ho, 2016).

The objective of this study was to define the correlation of BBR bioactivation with its hepatotoxicity by manipulating the structure of BBR. The correlation study was achieved by 1) structural modification of BBR through introducing halogen atoms to benzofuran ring at C6 position which is known to be a site of CYP3A metabolism; 2) evaluation of metabolic activation and toxicity of the test compounds; 3) determination of metabolic stability and pharmacokinetic properties; and 4) assessment of the efficacies of the new compounds *in vitro* and *in vivo*.

DMD Fast Forward. Published on October 11, 2017 as DOI: 10.1124/dmd.117.077818
This article has not been copyedited and formatted. The final version may differ from this version.

Materials and Methods

1. Reagents

Benzbromarone (BBR, >98%) and potassium oxonate (PO) were purchased from Aladdin Industrial Technology Co., Ltd. (Shanghai, China). 6-F-, Cl-, or Br-BBR (Figure 1) were synthesized in our laboratory (see Supplemental Methods for synthesis details). Buthionine sulfoximine (BSO, >99%), *N*-acetyl cysteine (NAC, >98%) and reduced nicotinamide adenine dinucleotide phosphate (NADPH) were acquired from Sigma-Aldrich (St. Louis, MO). [8-^{14}C]-Urate was obtained from American Radiolabled Chemicals (St. Louis, MO). Liquid scintillation was acquired from American Perkin Elmer Corporation. All organic solvents and reagents were of either analytical grade obtained from Fisher Scientific (Springfield, NJ) or HPLC grade from commercial sources.

2. Assay to measure the uricosuric effect in MDCK cells over-expressing hURAT1

Cell culture. Madin-Darby Canine Kidney (MDCK) cells with over-expressed hURAT1 were pre-prepared in our laboratory as described in our published work [32]. Cells were cultured in Dulbecco's modified Eagle's medium (DMEM) containing 10% fetal bovine serum, streptomycin (100 mg/mL), and penicillin (100 units/mL) in an atmosphere of 5% CO_2 and 95% air at 37 ℃.

[^{14}C]-Urate uptake experiment in MDCK-hURAT1 cells. Uptake assay was performed as described previously with several modifications (Wu et al., 2017). Briefly, cells were seeded in 24-well plates at a density of 1×10^5 cells/well. After 48

h, the culture medium was removed, and the resulting cells were washed three times with uptake buffer (125 mM sodium gluconate, 4.8 mM potassium gluconate, 1.3 mM calcium gluconate, 1.2 mM KH_2PO_4, 1.2 mM $MgSO_4$, 5.6 mM glucose, and 25 mM HEPES, pH=7.4). The cells were then incubated in another 0.5 mL of uptake buffer for 10 min at 37 ℃. Then the uptake buffer was removed, followed by addition of 200 μL of the medium containing [^{14}C]-Urate (25 μM) with or without the test compounds to initiate the uptake process. The test compounds were dissolved in DMSO and diluted with the culture medium to the final concentration of DMSO at < 1‰. The uptake step was set for 2 min and terminated by mixing with 0.6 mL of ice-cold dulbecco's phosphate buffered saline (DPBS) in wells. The resultant cells were washed with 1 mL of DPBS two times quickly, and then solubilized in 100 μL of 0.1M NaOH. The radioactivity of the cell lysates was determined by a liquid scintillation counter (Micro Beta2, PerkinElmer, Waltham, MA).

3. Animals

Male Sprague Dawley rats (200 ± 20 g) and male Kunming mice (20 ± 2 g) were purchased from the Animal Center of Shenyang Pharmaceutical University (Shenyang, China). Animals were housed in a controlled environment (temperature 25 ℃ and 12-h dark/light cycle) with free access to food and water. Animals were fasted overnight and tap water ad libitum prior to the experiments. The protocol of the animal experiments was approved by the Ethics Review Committee for Animal Experimentation of Shenyang Pharmaceutical University.

4. Assay to determine the uricosuric effect in hyperuricemic rats

Hyperuricemia was induced in rats using uricase inhibitor potassium oxonate (PO), according to previous reports (Haidari et al., 2012; Kou et al., 2016; Wang et al., 2016). Briefly, rats were intraperitoneally (i.p.) treated with potassium oxonate 1 h before the final administration of the test compounds. Animals were randomly allocated into six groups (n = 8). Groups I and II served as a healthy control and hyperuricemic control, respectively. Group III was hyperuricemic rats treated with BBR, which served as the positive control. Groups IV-VI consisted of hyperuricemic rats dosed with 6-F-, Cl-, or Br-BBR. The animals were administered (p.o.) with BBR or the other test compounds suspended in 0.9% CMC-Na at 10 mg/kg once daily for 8 days. On the eighth day, PO suspended in 0.9% saline solution was injected i.p. at 250 mg/kg 1 h in the resulting animals before the final administration of the test compounds. Blood samples were collected from the retro-orbital sinus 2 h after PO administration for the assessment of serum uric acid (SUA) levels. The blood samples were allowed to clot for 1 h at room temperature and then were centrifuged (8,000g, 4 ℃) for 10 min to obtain sera. The concentrations of SUA were determined spectrophotometrically using a commercially available standard diagnostic kit, according to manufacturers' instruction (Nanjing Jiancheng Technology Co., LTD, Nanjing, China).

5. Assessment of hepatotoxicities of BBR and 6-F-BBR

Male Kunming mice were randomly assigned into six groups (n = 4). Two groups of mice were p.o. treated with BBR or 6-F-BBR dissolved in 0.9% CMC-Na at

DMD Fast Forward. Published on October 11, 2017 as DOI: 10.1124/dmd.117.077818
This article has not been copyedited and formatted. The final version may differ from this version.

dose of 50 mg/kg for 7 consecutive days. Another two groups of mice were i.p. treated with BSO 1.5 h before the final administration of BBR or 6-F-BBR. Control groups treated with 0.9% CMC-Na or BSO were included. Blood samples were collected by cardiac puncture 24 h after the final administration. After clotting at room temperature for 3 h, the blood samples were centrifuged at 8,000 g for 10 min at 4 ℃. The resulting sera were collected for the determination of alanine transaminase (ALT) and aspartate transaminase (AST) activities on a VITROS 5600 Integrated System (Ortho-Clinical Diagnostics, Rochester, NY).

6. Metabolic stability test

Mouse liver microsomes (MLMs) and rat liver microsomes (RLMs) were prepared in our laboratory by following the protocol we previously published (Lin et al., 2007). Human liver microsomes (HLMs) were acquired from BD Gentest (Woburn, MA).

BBR or 6-F-BBR at a concentration of 1 μM or 10 μM was incubated with MLMs, RLMs, or HLMs (1 mg/mL), and $MgCl_2$ (3.2 mM) in a final volume of 0.5 mL of potassium phosphate buffer (0.1 M, pH 7.4). The mixture was preincubated at 37 ℃ for 3 min and then the reaction was commenced by addition of 1.0 mM NADPH. Aliquots of 50 μL were withdrawn at time points of 0, 5, 10, 15, 20, 30, and 60 min, and the reaction was immediately quenched by adding equal volume of ice-cold acetonitrile containing *S*-hexylglutathione (1.28 μM) as an internal standard. The samples were then vortex-mixed and spun at 16,000 g for 10 min at 4 ℃. The resulting supernatants (5 μL) were subjected to liquid chromatography-tandem mass

DMD Fast Forward. Published on October 11, 2017 as DOI: 10.1124/dmd.117.077818
This article has not been copyedited and formatted. The final version may differ from this version.

spectrometry (LC-MS/MS) for the analysis of the depletion of the compound. Each stability analysis was performed in triplicate. Natural log of the area ratio was plotted against the incubation time using GraphPad Prism 5 (San Diego, CA, USA), and the elimination rate constant (−k, the slope of the linear regression) was used to determine the *in vitro* half-life ($t_{1/2}$). For compounds with $t_{1/2}$ < 60 min, the *in vitro* intrinsic clearance (CL_{int}) was calculated as:

$$CL_{int} = \frac{-k}{[E]} \quad (1)$$

where [E] is the concentration of microsomal protein used in the incubation.

7. Metabolic activation studies of BBR and 6-F-BBR in liver microsomes

The incubation mixtures contained 1.0 mg of protein/mL MLMs, 3.2 mM $MgCl_2$, 75 μM BBR or 6-F-BBR, and 40 mM NAC in a final volume of 0.5 mL of phosphate buffer (pH 7.4). The reactions were initiated by addition of 1.0 mM NADPH and quenched by adding 0.5 mL of ice-cold acetonitrile after 60 min incubation at 37 ℃. Control incubations containing no NADPH were included. The reaction mixtures were vortex-mixed for 2 min, followed by centrifugation at 16,000 g for 10 min to remove precipitated protein. The resulting supernatants were concentrated by N_2 flushing at 40 ℃ and then redissolved in 100 μL of 50% acetonitrile in water. A 5 μL aliquot of the supernatants was injected into the LC-MS/MS system for analysis.

8. Determination of *in vivo* protein adductions derived from BBR and 6-F-BBR

Mice were treated i.p. with BBR or 6-F-BBR at 50 mg/kg. Liver tissues (0.2 g) harvested 30 min post administration were homogenized in 2.0 mL of phosphate

buffer (pH 7.4). The resulting homogenates were denatured by heating in a water bath at 60 ℃ for 30 min and then digested overnight with a mixture of chymotrypsin (1.0 mg/mL) and Pronase E (2.0 mg/mL), according to our early study (Wang et al., 2016b). The supernatants (5 μL) were subjected to the LC-MS/MS system for analysis.

9. Assessment of GSH level

Male Kunming mice were randomly divided into two groups (n = 4), and exposed i.p. to 50 mg/kg BBR or 6-F-BBR dissolved in corn oil. Plasma and liver samples were harvested post the administration at time of 0, 10, 30 min and 1, 2, 4, 8, 12 h. The liver tissues (0.2 g) were homogenized in 2.0 mL of phosphate buffer (0.1 M, pH 7.4). The assessment of plasma and hepatic GSH was achieved by monobromobimane (mBrB) derivatization as described in our published method (Yu et al., 2015), followed by the analysis of mBrB-GSH conjugate by LC-MS/MS.

10. Pharmacokinetic studies

Rats were randomly allocated into two groups (n = 6) and administered orally with the test compounds (BBR or 6-F-BBR) suspended in 0.9% CMC-Na by gavage at 10 mg/kg. Blood samples were collected from the retro-orbital sinus at 0 and 30 min as well as 1, 1.5, 2, 3, 4, 5, 6, 7, 8, 10, 12, and 24 h after dosing. The collected blood samples were centrifuged (8,000g, 4 ℃) for 10 min to obtain the plasma. Aliqouts (30 μL) of plasma were mixed with ice-cold acetonitrile (90 μL) containing *S*-hexylglutathione (1.28 nM) as an internal standard. The resulting mixtures were

DMD Fast Forward. Published on October 11, 2017 as DOI: 10.1124/dmd.117.077818
This article has not been copyedited and formatted. The final version may differ from this version.

vortex-mixed and centrifuged (16,000g, 4 ℃) for 10 min to remove the precipitated protein. Aliquots (2 μL) of the supernatants were subjected to the LC-MS/MS system for quantification of plasma BBR or 6-F-BBR, using validated specific and sensitive LC–MS/MS methods. Both the LLOQs of LC-MS/MS methods for BBR and 6-F-BBR were found to be 0.5 μg/mL.

11. LC-MS/MS Method

An AB SCIEX Instruments 5500 triple quadrupole (Applied Biosystems, Foster City, CA) equipped with an Agilent 1260 Series Rapid Resolution LC system (Agilent Technologies, Santa Clara, CA) was employed for the LC-MS/MS analyses. Samples were analyzed by multiple-reaction monitoring (MRM) scanning in electrospray ionization positive ion mode (ESI^+) using the following conditions: an ion-spray voltage of 5500 V; source temperature, 650 ℃; curtain gas (CUR), 35 psi; ion source gas 1 (GS1), 50 psi; ion source gas 2 (GS2), 50 psi. The parameters of ion pairs (declustering potential, DP; collision energy, CE; collision cell exit potential, CXP) were *m/z* 425→279 (110, 35, 3) for BBR, *m/z* 443→279 (110, 35, 3) for 6-F-BBR, *m/z* 392.2→246.3 (86, 24, 5) for *S*-hexylglutathione, *m/z* 586→279 (110, 35, 15) for BBR-NAC conjugate derived from epoxide (A1), *m/z* 544→279 (110, 25, 10) for cysteine-based protein adduction by epoxide metabolite(s) of BBR (A2), and *m/z* 498.2→192.2 (115, 50, 3) for mBrB-GSH conjugate. For the analysis of plasma BBR and 6-F-BBR concentrations, A1, A2, and mBrB-GSH conjugate, the mobile phase programs and the columns used were in accordance with our published studies (Wang et al., 2016a; Wang et al., 2016b). Data were processed using Applied

Biosystems/SCIEX Analyst software version 1.6.2.

12. Statistical analysis

Pharmacokinetic parameters were calculated from the mean plasma concentration by non-compartmental model, using Drug and Statistic (DAS) 2.1.1 software (Mathematical Pharmacology Professional Committee of China, Shanghai, China). Statistical analyses were performed using a Student's t-test. *($p < 0.05$), **($p < 0.01$) or ***($p < 0.001$) were considered significant.

Results

1. Characterization of 6-F-, Cl-, or Br-BBR

The general route for the synthesis of 6-F-, Cl-, or Br-BBR (Figure 1) is shown in Supplemental Scheme 1. The synthesis started with anhydrous magnesium chloride-catalyzed formylation of the corresponding 3-halogenated phenol with paraformaldehyde to produce halogenated salicylaldehyde **a**. Compound **a** was then cyclized with chloroacetone under the catalysis of KOH to give compound **b**, followed by Wolff-Kishner-Huangminglong reduction, Friedel-Crafts acylation, demethylation, and dibromination to give the final compounds. The C6-fluorinated, -chlorinated, and -brominated BBR, named 6-F-BBR, 6-Cl-BBR, and 6-Br-BBR respectively, were characterized by ^{1}H NMR, ^{13}C NMR (Figure 2 and 3**)** and HRESIMS (Figure 4). The ^{1}H NMR spectra depict the exact integration and the position of each proton present in the individual compounds. The ^{13}C NMR spectra show the position of carbons pertaining to each compound. The HRESIMS spectra display the deprotonated molecular ions $[M-H]^-$ with the representative isotope abundance patterns.

2. [^{14}C]-Urate uptake in MDCK-hURAT1 cells

hURAT1-transgenic MDCK cells were used to measure the amounts of [^{14}C]-Urate taken up for BBR, 6-F-BBR, 6-Cl-BBR, and 6-Br-BBR. As shown in Figure 5, BBR and 6-F-BBR at the concentration of 1 μM exhibited 59.39% and 63.59% inhibition of the uptake, respectively, compared with that of control. However, little inhibition was observed at the same concentration for 6-Cl-BBR and

6-Br-BBR. Even at the concentration of 15 μM, 6-Cl-BBR and 6-Br-BBR only showed weak inhibition of the uptake (21.72% and 13.33%, respectively). Clearly, 6-F-BBR, with similar efficacy as BBR, was a more potent hURAT1 inhibitor than 6-Cl-BBR and 6-Br-BBR.

3. Uricosuric efficacy in hyperuricemic rats

The effects of the test compounds on SUA levels were evaluated in potassium oxonate-induced hyperuricemic model rats. As shown in Table 1, after 7 day treatment with BBR or the test compounds, SUA levels in each group were significantly reduced ($p < 0.001$, 0.001, 0.01, and 0.01 respectively), compared with the normal control. There was no significant difference between BBR and 6-F-BBR in lowering the SUA levels of healthy rats. As expected, intraperitoneally administration of oxonate significantly ($p < 0.001$) elevated SUA levels compared with that of the normal control. In addition, the groups treated with BBR, 6-F-, Cl-, or Br-BBR all demonstrated significantly lower levels of SUA ($p < 0.001$, 0.001, 0.01, and 0.01 respectively), compared with the hyperuricemic control. However, the decreased levels of SUA achieved by 6-F-BBR were comparable to that of BBR, which made us select 6-F-BBR as the lead uricosuric benzofuran derivative. As a result, a thorough comparative study on metabolism and toxicities of BBR and 6-F-BBR was carried out as follows.

4. Hepatotoxicities of BBR and 6-F-BBR

The hepatotoxicities of BBR and 6-F-BBR were evaluated by the assessment of

serum ALT and AST activities in mice. Administration of BBR by oral gavage at 50 mg/kg for 7 consecutive days caused significant elevation of serum AST activity in mice 24 h after the final administration, compared with that in vehicle-treated animals ($p < 0.01$) and 6-F-BBR-treated animals ($p < 0.05$). A minor increase in serum ALT activity was observed in animals treated with BBR but without statistical difference, compared with that of vehicle-treated animals. In a separate study, the hepatotoxicities of BBR and 6-F-BBR were examined in mice pretreated with BSO 1.5 h before the final administration. Pretreatment with BSO was found to potentiate 6-F-BBR- and BBR-induced elevation of serum ALT and AST. However, the elevations of ALT and AST induced by BBR were significantly higher than those induced by 6-F-BBR (Figure 6). Both studies demonstrated that 6-F-BBR was less hepatotoxic than BBR.

5. Metabolic stability

Metabolic stability of BBR and 6-F-BBR was examined in mouse, rat, and human liver microsomes. The substrates all decayed in mono-exponential manners (Supplemental Figure 1) in microsomes. As shown in Table 2, 50% of BBR at 1.0 μM was metabolized in mouse, rat, and human liver microsomes in 5.6 4.2, and 8.6 min. However, the half life of 6-F-BBR in the microsomes was > 60, 8.4, and 13.6 min, respectively. At the concentration of 10 μM, similar increased metabolic stability for 6-F-BBR was observed in the microsomes. Taken together, 6-F-BBR was much more stable in the microsome tests than BBR, and the introduction of a 6-fluoro substituent on the benzofuran ring (6-F-BBR vs BBR) offered resistance

DMD Fast Forward. Published on October 11, 2017 as DOI: 10.1124/dmd.117.077818
This article has not been copyedited and formatted. The final version may differ from this version.

against the metabolism.

6. *In vitro* metabolism (epoxidation) of BBR and 6-F-BBR

Our early study demonstrated that epoxide metabolite(s) was a primary reactive metabolite of BBR which may be related to BBR hepatotoxicity (Wang et al., 2016a). The potentials of metabolic activation (epoxidation) of BBR and 6-F-BBR were evaluated in mouse liver microsomes supplemented with NAC as a trapping agent. The representative chromatograms of NAC conjugate derived from epoxide metabolite(s) of BBR and 6-F-BBR are shown in Figure 7. As expected, only minor epoxide-derived NAC conjugate (**A1**, Scheme 1) was detected in 6-F-BBR-supplemented microsomal incubations. Apparently, an approximately 300-fold more **A1** was produced in microsomal incubation of BBR. In addition, we failed to detect the corresponding NAC conjugate derived from 6-F-BBR, indicating that no epoxide metabolites were formed in the metabolism of 6-F-BBR and that the introduction of fluorine atom to BBR deactivated the aromatic ring towards epoxidation.

7. Epoxide-derived hepatic protein modification by BBR and 6-F-BBR

The detection of epoxide-derived liver protein covalent binding in 6-F-BBR- or BBR-treated mice was achieved by proteolytic digestion of the protein adducts to the corresponding cysteine conjugates. The representative chromatograms of the cysteine adducts are shown in Figure 8. Epoxide-derived cysteine adduct **A2** (Scheme 1) was detected in BBR-treated mice, while no such adduct was observed in

mice given 6-F-BBR.

8. Hepatic and plasma GSH depletion induced by BBR and 6-F-BBR in mice

Depletion of cellular GSH has been considered as a biomarker for the production of reactive metabolites and early stage of cell injury. Time courses of hepatic and plasma GSH levels were monitored in 6-F-BBR- and BBR-treated mice (Figure 9). Hepatic and plasma GSH were dramatically depleted as much as 87 % and 92 %, respectively, in mice after a hepatotoxic dose (50 mg/kg) of BBR, while 6-F-BBR demonstrated much less potential to deplete hepatic and plasma GSH than BBR at the same dose.

9. Pharmacokinetic behaviors

Plasma BBR and 6-F-BBR were monitored in rats given a single dose of BBR or 6-F-BBR at 10 mg/kg by oral gavage. The concentration-time (0-24 h) curves of the compounds are shown in Figure 10, and the corresponding pharmacokinetic parameters are presented in Table 3. Both BBR and 6-F-BBR revealed double-peak property in their pharmacokinetic profiles. 6-F-BBR achieved a C_{max} (54.59 μg/mL) and AUC (256.20 μg/mL ħ) as over twice as those of BBR-treated animals (26.80 μg/mL and 123.66 μg/mL ħ, respectively). In addition, with the observed good metabolic stability in RLMs, 6-F-BBR displayed a much lower *in vivo* clearance (0.04 L/h/kg) than that of BBR (0.09 L/h/kg). There was no significant difference in half-life between BBR (3.86 h) and 6-F-BBR (2.59 h).

Discussion

Though BBR shows great potential in the treatment of gout, it has not been licensed for use in Europe, due to several reports of fatal idiosyncratic hepatic failure. Idiosyncratic toxicities are considered to be associated with metabolic activation of pro-toxicants. Our early study demonstrated that CYP3A-mediated epoxidation of BBR at benzofuran ring was related to BBR-induced protein adduction and hepatotoxicity (Wang et al., 2016a; Wang et al., 2016b). To avoid metabolic activation-induced liver injury by BBR, we replaced the hydrogen at the metabolically labile site with a halogen atom, which is a commonly used strategy to attenuate the potential of P450-mediated metabolism (metabolic activation). Currently, 50% of leading drugs on the pharmaceutical market are halogenated (Xu et al., 2014), and there is a great potential to exploit halogens into drug design in medicinal chemistry.

In this study, three BBR derivatives substituted with a halogen (F, Cl, or Br) at C6 of BBR, the site of epoxidation catalyzed by CYP3A, were designed and synthesized to block the metabolic activation of BBR. As the initial step, we evaluated the uricosuric efficacy of the resulting compounds (6-F-, Cl-, or Br-BBR) to identify the most effective compound for further toxicity and metabolism investigation. The efficacy evaluation started with assessment of inhibitory effect on urate transport in hURAT1-transgenic cells, since uricosuric BBR is known to be a potent inhibitor of hURAT1. 6-F-BBR was found to inhibit hURAT1 the most, followed by BBR, 6-Cl-BBR, and 6-Br-BBR in order. In addition, we evaluated their suppressive effects on SUA in rats with hyperuricemia (Table 1). No statistical

significance was observed in SUA levels in healthy rats treated with 6-F-, Cl-, or Br-BBR, presumably due to the protective compensation reaction of healthy rats. However, 6-F-BBR elicited more potency to decrease SUA level than 6-Cl-BBR ($p < 0.001$) and 6-Br-BBR ($p < 0.05$) in hyperuricemic rats. Both *in vitro* and *in vivo* studies demonstrated that fluorinated BBR (6-F-BBR) was as effective as BBR and more effective than the chlorinated and brominated BBR (6-Cl-BBR and 6-Br-BBR). The observed favorable efficacy of 6-F-BBR was possibly attributed to the highly electronegative nature of fluorine, the similarity in size of hydrogen (BBR) as that of fluorine (fluorinated BBR), along with the low polarizability of fluorine (Hernandes et al., 2010). These chemical characteristics of fluorine can productively influence physicochemical and conformational properties of 6-F-BBR, which may contribute to the improvement in oral absorption in rats (Table 3). As a result, this makes 6-F-BBR present dominated pharmacological properties.

As the core of the present study, hepatotoxicities of BBR and 6-F-BBR were evaluated *in vivo*. We succeeded in development of a mouse model for the assessment of hepatotoxicities of BBR and 6-F-BBR in mice pretreated with BSO. BSO is known to have an ability to deplete GSH contents by inhibiting γ-glutamylcysteine synthetase, a rate-limiting enzyme in the biosynthesis of GSH. Significant elevations of serum ALT and AST were observed in BSO-pretreated mice given BBR, while a minor or slight increase in serum ALT and AST was found in animals treated with BBR alone (Figure 6). This made it possible to evaluate the hepatotoxicity of BBR and hopefully its idiosyncratic liver injury, although the

mechanisms of the development of idiosyncratic toxicity remain unknown.

6-F-BBR was selected for further hepatotoxicity and metabolic activation evaluation, since the fluorinated BBR was found to be the most effective uricosurics among the compounds tested and be as effective as BBR (Table 1 and Figure 5). The toxicity study was performed in mice pretreated with BSO. 6-F-BBR was found to be much less hepatotoxic than BBR (Figure 6). The metabolism study demonstrated that the metabolic activation (epoxidation) of 6-F-BBR was almost abolished. Microsomal incubations of 6-F-BBR fortified with NAC revealed a significant decrease in the formation of epoxide-derived NAC conjugate by nearly 99.7% compared with that of BBR, and no epoxide-derived protein adduction was detected in mice given 6-F-BBR (Figures 7 and 8). It is likely that the introduced fluorine blocked the site from metabolic epoxidation. Additionally, the electron withdrawing effect of the fluorine decreased the electron density of the phenyl ring, which disfavors the oxidation reaction. The observation of high volume of protein adduction derived from BBR, combined with the finding of more potent hepatotoxicity induced by BBR, led us to propose that epoxidation at C6 of BBR is a key step for hepatotoxicity of BBR.

Our previous study demonstrated that the reaction of the epoxide metabolite(s) of BBR with GSH contributes to the depletion of GSH (Wang et al., 2016b). The present study found that treatment of BBR caused significant elevation in serum AST activity in opposition to decrease in hepatic and plasma GSH content. On the contrary, slight hepatotoxicity, along with attenuated GSH depletion, was observed in

mice given 6-F-BBR, indicating that the formation of the epoxide metabolite(s) was slowed down by fluorine substitution. It should be noted that 6-F-BBR did not protect mice completely from GSH depletion. A decrease of GSH level was also observed during the first 30 min post administration of 6-F-BBR. This might result from the formation of catechol (Scheme 1) and hydroquinone through *ipso*-substitution of the dibromophenol ring (Kitagawara et al., 2015). We cannot underestimate possible contribution of their oxidized forms (quinone metabolites, data unpublished) which are known to be able to deplete GSH. The observed attenuated GSH depletion at least partially resulted from the fluorine substitution. The supporting evidence was that little metabolites derived from the epoxidation of 6-F-BBR were observed.

6-F-BBR was more stable than BBR in liver microsomes, particularly in mouse liver microsomes (as much as 10-fold more stable, Table 2). This indicates that the incorporation of fluorine kept the molecule from P450-mediated metabolism. It is believed that the electron-withdrawing property of the fluorine substituent deactivated the aromatic system towards metabolic degradation by P450 enzymes. Besides epoxidation of BBR at benzofuran ring, BBR was suggested to be oxidized to a quinone metabolite via sequential oxidation of 6-OH-BBR (McDonald and Rettie, 2007). Additionally, Naoki and coworkers demonstrated that BBR was metabolized to a quinone methide derived from 1′,6-dihydroxy BBR (Cho et al., 2017). We failed to detect the formation of such reactive metabolites directly from BBR in liver microsomal systems, indicating that the two metabolic pathways are minor in

comparison with the epoxidation. The observed improvement of 6-F-BBR metabolic stability probably resulted mainly from retarding of the epoxidation of the benzrofuran ring, and unlikely from that of the two minor pathways.

The metabolic stability studies demonstrated that the $t_{1/2}$ of 6-F-BBR increased twice as many as that of BBR in RLMs, and over two-fold increases in C_{max} and AUC values were observed in 6-F-BBR-treated rats relative to those of animals treated with BBR at the same dose. This might result from the improvement of oral absorption, presumably due to the increase of membrane permeability by fluorine substitution. Permeability is one of the major considerations in the lead optimization of oral drugs. Many drugs with aromatic fluorination are prone to penetrate cell membranes, thereby increasing the intracellular concentration (Smart, 2001; Murphy and Sandford, 2015). Furthermore, 6-F-BBR was much more stable than BBR in MLMs with $t_{1/2} > 60$ min. It might be reasonable to assume that exposures of 6-F-BBR would be greater than that of BBR in mice. Surprisingly, 6-F-BBR displayed much lower hepatotoxicity than BBR (Figure 6). This suggests that the observed toxicity of BBR was induced by its metabolite but not the parent compound itself. Interestingly, with the observed good metabolic stability in RLMs, 6-F-BBR displayed a slightly increased elimination rate than that of BBR *in vivo* (Figure 10). Explanation for the observed discrepancy could arise from elevated phase Ⅱ metabolism, such as glucuronidation or sulfation, involved in biotransformation of 6-F-BBR. The resulting polar conjugates could be eliminated quickly.

Conclusively, replacement of the hydrogen in the metabolically labile site by a

fluorine atom significantly attenuated the hepatotoxicity of BBR but did not alter its uricosuric efficacy. The present work provided a solid evidence that the formation of the epoxide(s) is a key step for the development of BBR-induced hepatotoxicity. Additionally, the fluorinated BBR was identified as effective as BBR, and this study is an excellent example of drug metabolism-guided rational drug design.

Authorship Contributions:

Participated in research design: Zheng, S.J. Wang, and Pang.

Conducted experiments: H. Wang, Peng, Zhang, Lan, Y.F. Zhao, and X. Wang.

Performed data analysis: H. Wang, H.M. Zhao, W.B. Wang, and Peng.

Wrote or contributed to the writing of the manuscript: H. Wang and Zheng.

References

Abhishek A, Roddy E, and Doherty M (2017) Gout-a guide for the general and acute physicians. *Clin Med (Lond)* **17**: 54-59.

Ahn SO, Ohtomo S, Kiyokawa J, Nakagawa T, Yamane M, Lee KJ, Kim KH, Kim BH, Tanaka J, Kawabe Y, and Horiba N (2016) Stronger uricosuric effects of the novel selective URAT1 inhibitor UR-1102 lowered plasma urate in tufted capuchin monkeys to a greater extent than benzbomarone. *J Pharmacol Exp Ther* **357**: 157-166.

Arai M, Yokosuka O, Fujiwara K, Kojima H, Kanda T, Hirasawa H, and Saisho H (2002) Fulminant hepatic failure associated with benzbromarone treatment: a case report. *J Gastroenterol Hepatol* **17**: 625-626.

Bacsa I, Jójárt R, Schneider G, Wölfling J, Maróti P, Herman BE, Szécsi M, and Mernyák E (2015) Synthesis of A-ring halogenated 13α-estrone derivatives as potential 17β-HSD1 inhibitors. *Steroids* **104**: 230-236.

Baker JF and Schumacher HR (2010) Update on gout and hyperuricemia. *Int J Clin Pract* **64**: 371-377.

Byun JH, Kim H, Kim Y, Mook-Jung I, Kim DJ, Lee WK, and Yoo KH (2008) Aminostyrylbenzofuran derivatives as potent inhibitors for Abeta fibril formation. *Bioorganic & Medicinal Chemistry Letters* **18**: 5591-5593.

Cho N, Kobayashi K, Yoshida M, Kogure N, Takayama H, and Chiba K (2017) Identification of novel glutathione adducts of benzbromarone in human liver microsomes. *Drug Metab Dispos* **32**: 46-52.

Choi HK, Mount DB, and Reginato AM (2005) Pathogenesis of gout. *Ann Intern Med* **143**: 499-516.

Dekker SJ, Zhang Y, Vos JC, Vermeulen NP, and Commandeur JN (2016) Different reactive metabolites of nevirapine require distinct glutathione S-transferase isoforms for bioinactivation. *Chem Res Toxicol* **29**: 2136-2144.

Doherty M (2009) New insights into the epidemiology of gout. *Rheumatology (Oxford)* **48 Suppl 2**: ii2-ii8.

Fernandes EA, Bergamaschi SB, Rodrigues TC, Dias GC, Malmann R, Ramos GM, and Monteiro SS (2016) Relevant aspects of imaging in the diagnosis and management of gout. *Rev Bras Reumatol* doi: 10.1016/j.rbr.2016.03.006.

Ford MC and Ho PS (2016) Computational tools to model halogen bonds in medicinal chemistry. *J Med Chem* **59**: 1655-1670.

Haidari F, Rashidi MR, and Mohammad-Shahi M (2012) Effects of orange juice and hesperetin on serum paraoxonase activity and lipid profile in hyperuricemic rats. *Bioimpacts* **2**: 39-45.

Hernandes MZ, Cavalcanti SM, Moreira DR, de Azevedo Junior WF, and Leite AC (2010) Halogen atoms in the modern medicinal chemistry: hints for the drug design. *Curr Drug Tragets* **11**: 303-314.

Hu K and Jeong JH (2006) A convergent synthetic study of biologically active benzofuran derivatives. *Arch Pharm Res* **29**: 476-478.

Keenan RT and Schlesinger N (2016) New and pipeline drugs for gout. *Curr Rheumatol Rep* **18**: 32.

Kitagawara Y, Ohe T, Tachibana K, Takahashi K, Nakamura S, and Mashino T (2015) Novel bioactivation pathway of benzbromarone mediated by cytochrome P450. *Drug Metab Dispos* **43**:1303-1306.

Kou Y, Li Y, Ma H, Li W, Li R, and Dang Z (2016) Uric acid lowering effect of Tibetan Medicine RuPeng15 powder in animal models of hyperuricemia. *J Tradit Chin Med* **36**: 205-210.

Kydd AS, Seth R, Buchbinder R, Edwards CJ, and Bombardier C (2014) Uricosuric medications for chronic gout. *Cochrane Database Syst Rev* CD010457.

Lee MH, Graham GG, Williams KM, and Day RO (2008) A benefit-risk assessment of benzbromarone in the treatment of gout. Was its withdrawal from the market in the best interest of patients? *Drug Saf* **31**: 643-665.

Leung L, Kalgutkar AS, and Obach RS (2012) Metabolic activation in drug-induced liver injury. *Drug Metab Rev* **44**: 18-33.

Lin G, Tang J, Liu XQ, Jiang Y, and Zheng J (2007) Deacetylclivorine: a gender-selective metabolite of clivorine formed in female Sprague-Dawley rat liver microsomes. *Drug Metab Dispos* **35**: 607-613.

Lu Y, Wang Y, and Zhu W (2010) Nonbonding interactions of organic halogens in biological systems: implications for drug discovery and biomolecular design. *Phys Chem Chem Phys* **12**: 4543-4551.

McDonald MG and Rettie AE (2007) Sequential metabolism and bioactivation of the hepatotoxin benzbromarone: formation of glutathione adducts from a

catechol intermediate. *Chem Res Toxicol* **20**: 1833-1842.

Murphy CD and Sandford G (2015) Recent advances in fluorination techniques and their anticipated impact on drug metabolism and toxicity. *Expert Opin Drug Metab Toxicol* **11**: 589-599.

Obach RS, Walker GS, and Brodney MA (2016) Biosynthesis of fluorinated analogs of drugs using human cytochrome P450 enzymes followed by deoxyfluorination and quantitative nuclear magnetic resonance spectroscopy to improve metabolic stability. *Drug Metab Dispos* **44**: 634-646.

Patel MM and Bhat HK (2004) Differential oxidant potential of carcinogenic and weakly carcinogenic estrogens: involvement of metabolic activation and cytochrome P450. *J Biochem Mol Toxicol* **18**: 37-42.

Perez-Ruiz F, Dalbeth N, and Bardin T (2015) A review of uric acid, crystal deposition disease and gout. *Adv Ther* **32**: 31-41.

Purser S, Moore PR, Swallow S, and Gouverneur V (2008) Fluorine in medicinal chemistry. *Chem Soc Rev* **37**: 320-330.

Rizzo S, Rivière C, Piazzi L, Bisi A, Gobbi S, Bartolini M, Andrisano V, Morroni F, Tarozzi A, Monti JP, and Rampa A (2008) Benzofuran-based hybrid compounds for the inhibition of cholinesterase activity, beta amyloid aggregation, and abeta neurotoxicity. *J Med Chem* **51**: 2883-2886.

Rosenblum SB, Huynh T, Afonso A, Davis HR Jr, Yumibe N, Clader JW, and Burnett DA (1998) Discovery of 1-(4-fluorophenyl)-(3R)-[3-(4-fluorophenyl)-(3S)-hydroxypropyl]-(4S)-(4-

hydroxyphenyl-2-azetidinone (SCH 58235): a designed, potent, orally active inhibitor of cholesterol absorption. *J Med Chem* **41**: 973-980.

Ruoff G and Edwards NL (2016) Overview of serum uric acid treatment targets in gout: why less than 6 mg/dL? *Postgrad Med* **128**: 706-715.

Smart BE (2001) Fluorine substituent effects (on bioactivity). *J Fluor Chem* **109**: 3-11.

Smith EU, Díaz-Torné C, Perez-Ruiz F, and March LM (2010) Epidemiology of gout: an update. *Best Pract Res Clin Rheumatol* **24**: 811-827.

Uini UH and Lars S (1999) Convenient method for the ortho-formylation of phenols. *Acta Chemica Scandinavica* **53**: 258-262.

Wang H, Feng YK, Wang Q, Guo XC, Huang WL, Peng Y, and Zheng J (2016) Cysteine-based protein adduction by epoxide-derived metabolite(s) of benzbromarone. *Chem Res Toxicol* **29**: 2145-2152.

Wang K, Wang H, Peng Y, and Zheng J (2016) Identification of epoxide-derived metabolite(s) of benzbromarone. *Drug Metab Dispos* **44**: 607-615.

Wang WL, Sheu SY, Huang WD, Chuang YL, Tseng HC, Hwang TS, Fu YT, Kuo YH, Yao CH, and Kuo TF (2016) Phytochemicals from tradescantia albiflora kunth extracts reduce serum uric acid levels in oxonate-induced rats. *Pharmacogn Mag* **12**: S223-S227.

Wempe MF, Jutabha P, Quade B, Iwen TJ, Frick MM, Ross IR, Rice PJ, Anzai N, and Endou H (2011) Developing potent human uric acid transporter 1 (hURAT1) inhibitors. *J Med Chem* **54**: 2701-2713.

Wilcken R, Zimmermann MO, Lange A, Joerger AC, and Boeckler FM (2013) Principles and applications of halogen bonding in medicinal chemistry and chemical biology. *J Med Chem* **56**: 1363-1388.

Wu T, Chen JS, Dong S, Li HS, Cao Y, Tian YX, Fu WM , Zhou PZ, Xi BM, and Pang JX (2017) Identification and characterization of a potent and selective inhibitor of human urate transporter 1. *Pharmacol Rep* doi: http://dx.doi.org/doi:10.1016/j.pharep.2017.04.022.

Xu Z, Yang Z, Liu Y, Lu Y, Chen K, and Zhu W (2014) Halogen bond: its role beyond drug-target binding affinity for drug discovery and development. *J Chem Inf Model* **54**: 69-78.

Xuan J, Chen S, Ning B, Tolleson WH, and Guo L (2016) Development of HepG2-derived cells expressing cytochrome P450s for assessing metabolism-associated drug-induced liver toxicity. *Chem Biol Interact* **255**: 63-73.

Yu J, Li CY, Shen SJ, Liu XQ, Peng Y, and Zheng J (2015) Mass spectrometry based detection of glutathione with sensitivity for single-cell analysis. *Rapid Commun Mass Spectrom* **29**: 681-689.

Footnotes: This work was supported in part by the National Natural Science Foundation of China [Grants 81373471, 81430086, 81773813]; the Natural Science Foundation of Liaoning Province [Grant 2015020738]; and the Scientific Research Program of Hainan Province [Grant ZDYF2016143].

H. W. and Y. P. contributed equally to this work.

Legends for figures

Figure 1. Structures of BBR and 6-F-, Cl-, or Br-BBR.

Figure 2. Characterization of 6-F-BBR (**A**), 6-Cl-BBR (**B**) and 6-Br-BBR (**C**) by ^{1}H NMR analysis.

Figure 3. Characterization of 6-F-BBR (**A**), 6-Cl-BBR (**B**) and 6-Br-BBR (**C**) by ^{13}C NMR analysis.

Figure 4. Characterization of 6-F-BBR, 6-Cl-BBR and 6-Br-BBR by HRESIMS analysis. High-resolution mass spectra of 6-F-BBR (**A**), 6-Cl-BBR (**B**) and 6-Br-BBR (**C**) analyzed by micro Q-TOF MS (Bruker Corporation, Billerica, MA).

Figure 5. [^{14}C]-Urate uptake in MDCK-hURAT1 transgenic cells in the presence of BBR (1 μM), 6-F-BBR (1 μM), 6-Cl-BBR (15 μM) and 6-Br-BBR (15 μM). *p < 0.05, **p < 0.01, ***p < 0.001, compared with that of the control group.

Figure 6. Hepatotoxicities of BBR and 6-F-BBR. Mice were pretreated (i.p.) with BSO (666 mg/kg) 1.5 h before the final administration (p.o.) of BBR or 6-F-BBR (50 mg/kg) for 7 consecutive days. The groups of BBR or 6-F-BBR alone without BSO pretreatment as well as control groups treated with 0.9% CMC-Na or BSO were all included. Serum ALT and AST activities were examined 24 h after the final administration (n = 4). $^{*}p$ < 0.05, $^{**}p$ < 0.01, $^{***}p$ < 0.001 were considered significantly different from vehicle-treated group; $^{\#}p$ < 0.05, $^{\#\#\#}p$ < 0.001 were considered significantly different from 6-F-BBR-treated group.

Figure 7. Extracted ion chromatograms of MRM scan of *m/z* 586→279 obtained from the analysis of mouse liver microsomal incubations containing NAC and 6-F-BBR (**A**)

or BBR (**B**).

Figure 8. Extracted ion chromatograms of MRM scans of *m/z* 544→279 obtained from analysis of cysteine-based protein adduction of mice after 30 min administration (i.p.) of 6-F-BBR (**A**) and BBR (**B**) at 50 mg/kg.

Figure 9. Assessment of GSH contents in mouse liver (**A**) and plasma (**B**). Mice were treated (i.p.) with BBR or 6-F-BBR at 50 mg/kg. The assessment of GSH was achieved by mBrB derivatization and LC-MS/MS analysis. GSH levels were measured post the administration at time of 0, 10, 30, and 1, 2, 4, 8, 12 h. $*p < 0.05$, $**p < 0.01$, $***p < 0.001$ compared with that of BBR**.**

Figure 10. Time-course of plasma BBR and 6-F-BBR in rats after p.o. administration of BBR or 6-F-BBR at 10 mg/kg. Plasma BBR and 6-F-BBR were measured at time intervals of 0, 30 min and 1, 1.5, 2, 3, 4, 5, 6, 7, 8, 10, 12, and 24 h after administration. Data represent the mean ± SD, n = 6; $*p < 0.05$, $**p < 0.01$, $***p < 0.001$ compared with BBR**.**

Scheme 1. Proposed pathway of NAC conjugation, and protein and cysteine adduct formation derived from reactive metabolite(s) of BBR.

DMD Fast Forward. Published on October 11, 2017 as DOI: 10.1124/dmd.117.077818
This article has not been copyedited and formatted. The final version may differ from this version.

Table 1. Effects of BBR and 6-F-, Cl-, or Br-BBR on serum uric acid (SUA) levels in oxonate-induced hyperuricemic rats (mean ± SD, n = 8).

Groups	Dose (mg/kg)	7d	8d
		SUA	SUA
Normal control	—	76.4±6.2	75.4±4.6
Hyperuricemic control	—	74.7±4.8	254.1±21.2[a]
Hyperuricemic-BBR-treated	10	54.4±9.5[a]	172.2±20.8[d]
Hyperuricemic-6-F-BBR-treated	10	59.8±6.2[a]	186.4±14.7[d]
Hyperuricemic-6-Cl-BBR -treated	10	63.7±6.1[b,c]	222.4±18.4[c,e,f]
Hyperuricemic-6-Br-BBR -treated	10	64.3±5.5[b,c]	215.6±25.8[c,e,g]

[a] Compared with normal control group: $p < 0.001$.

[b] Compared with normal control group: $p < 0.01$.

[c] Compared with BBR-treated group: $p < 0.05$.

[d] Compared with hyperuricemic control group: $p < 0.001$.

[e] Compared with hyperuricemic control group: $p < 0.01$.

[f] Compared with hyperuricemic-6-F-BBR-group: $p < 0.001$.

[g] Compared with hyperuricemic-6-F-BBR-group: $p < 0.05$.

DMD Fast Forward. Published on October 11, 2017 as DOI: 10.1124/dmd.117.077818
This article has not been copyedited and formatted. The final version may differ from this version.

Table 2. Metabolic stability of BBR and 6-F-BBR in liver microsomes.

Compounds	Concentration	MLMs		RLMs		HLMs	
		$t_{1/2}$	CL_{int}	$t_{1/2}$	CL_{int}	$t_{1/2}$	CL_{int}
BBR	1 μM	5.6	0.124	4.2	0.163	8.6	0.081
	10 μM	10.9	0.064	11.3	0.061	>60	—
6-F-BBR	1 μM	>60	—	8.4**	0.082***	13.6*	0.051*
	10 μM	>60	—	15.1	0.046	>60	—

The units of $t_{1/2}$ and CL_{int} are min and mL/min/mg protein, respectively.

***p* < 0.05, ***p* < 0.01, and ****p* < 0.001 compared with that of BBR**.

DMD Fast Forward. Published on October 11, 2017 as DOI: 10.1124/dmd.117.077818
This article has not been copyedited and formatted. The final version may differ from this version.

Table 3. Summary of pharmacokinetic parameters obtained in rats after p.o. administration of BBR and 6-F-BBR[a].

parameters	BBR	6-F-BBR
C_{max} (μg/mL)	26.80 ± 11.19	54.59 ± 10.17[c]
T_{max} (h)	1.25 ± 0.27	1.75 ± 0.27[d]
$AUC_{(0-t)}$ (μg/mL ħ)	121.62 ± 39.20	245.35 ± 28.80[b]
$AUC_{(0-\infty)}$ (μg/mL ħ)	123.66 ± 38.41	256.20 ± 43.88[b]
CL/F (L/h/kg)	0.09 ± 0.03	0.04 ± 0.01[c]
$t_{1/2}$ (h)	3.86 ± 1.27	2.59 ± 0.55
Vz/F (L/kg)	0.52 ± 0.28	0.15 ± 0.02[d]

[a]10 mg/kg, n = 6.
[b]Significantly different from BBR-treated mice ($p < 0.001$).
[c]Significantly different from BBR-treated mice ($p < 0.01$).
[d]Significantly different from BBR-treated mice ($p < 0.05$).

DMD Fast Forward. Published on October 11, 2017 as DOI: 10.1124/dmd.117.077818
This article has not been copyedited and formatted. The final version may differ from this version.

Figure 1.

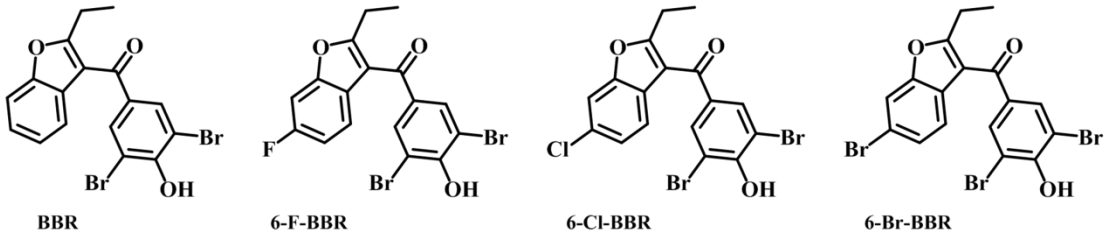

BBR 6-F-BBR 6-Cl-BBR 6-Br-BBR

DMD Fast Forward. Published on October 11, 2017 as DOI: 10.1124/dmd.117.077818
This article has not been copyedited and formatted. The final version may differ from this version.

Figure 2.

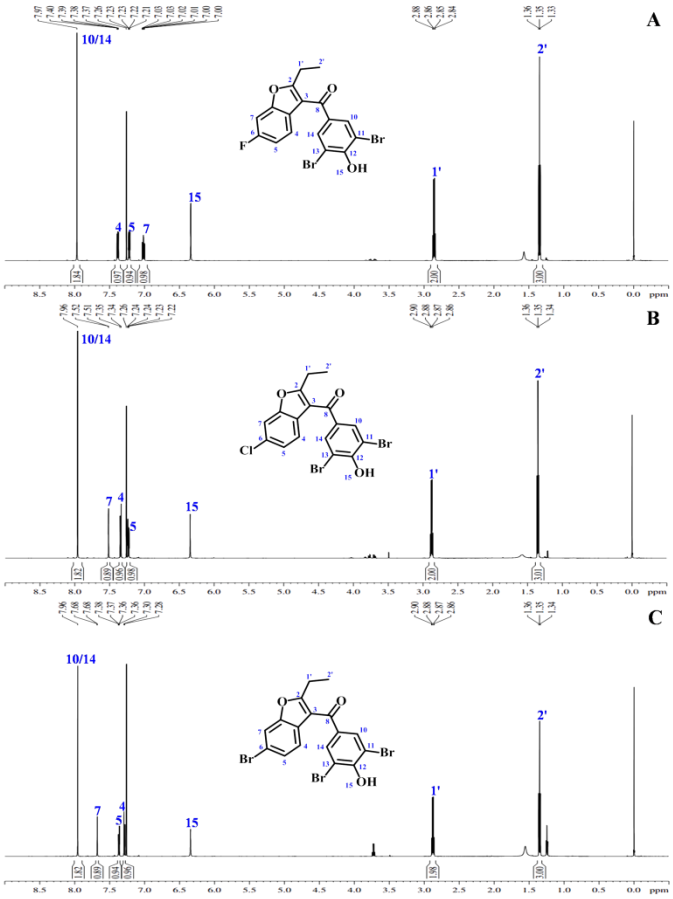

DMD Fast Forward. Published on October 11, 2017 as DOI: 10.1124/dmd.117.077818
This article has not been copyedited and formatted. The final version may differ from this version.

Figure 3.

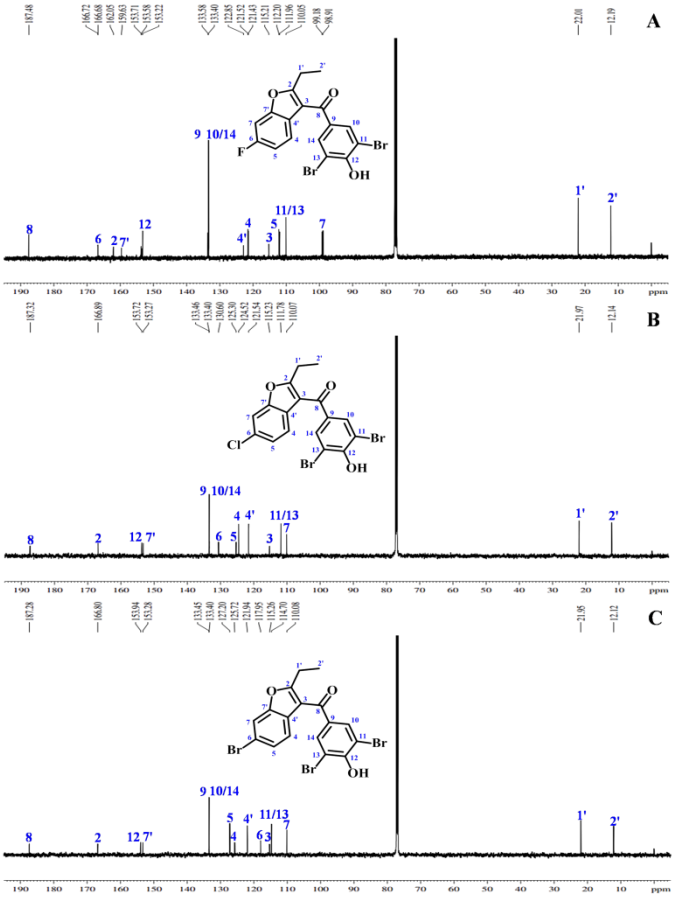

DMD Fast Forward. Published on October 11, 2017 as DOI: 10.1124/dmd.117.077818
This article has not been copyedited and formatted. The final version may differ from this version.

Figure 4.

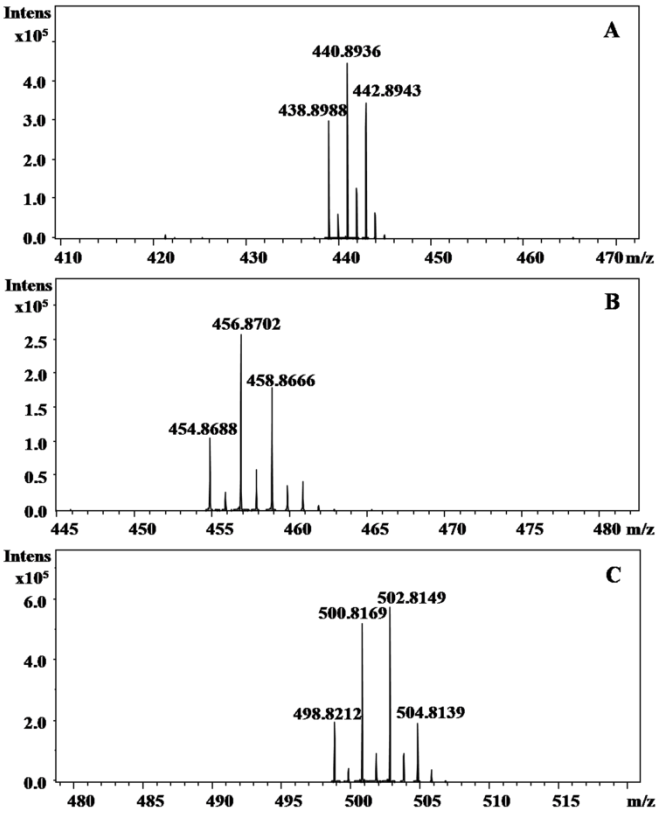

DMD Fast Forward. Published on October 11, 2017 as DOI: 10.1124/dmd.117.077818
This article has not been copyedited and formatted. The final version may differ from this version.

Figure 5.

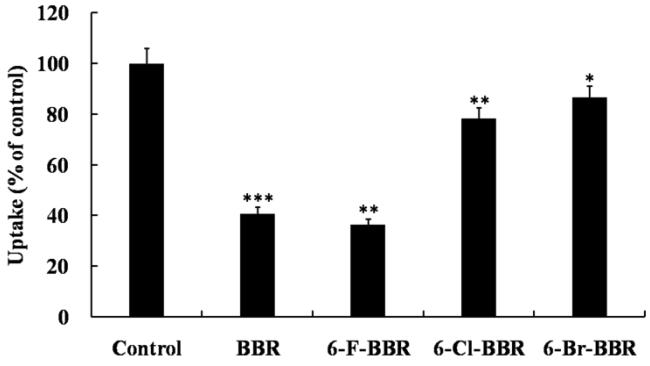

DMD Fast Forward. Published on October 11, 2017 as DOI: 10.1124/dmd.117.077818
This article has not been copyedited and formatted. The final version may differ from this version.

Figure 6.

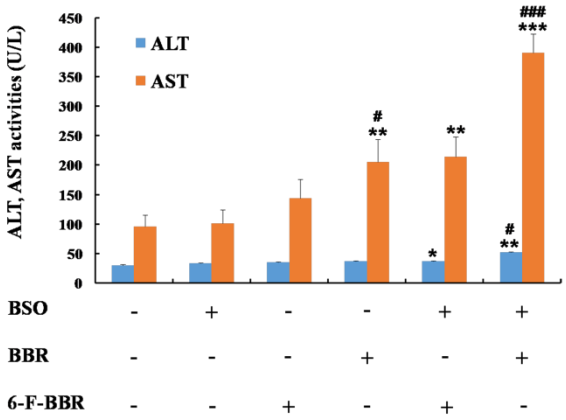

DMD Fast Forward. Published on October 11, 2017 as DOI: 10.1124/dmd.117.077818
This article has not been copyedited and formatted. The final version may differ from this version.

Figure 7.

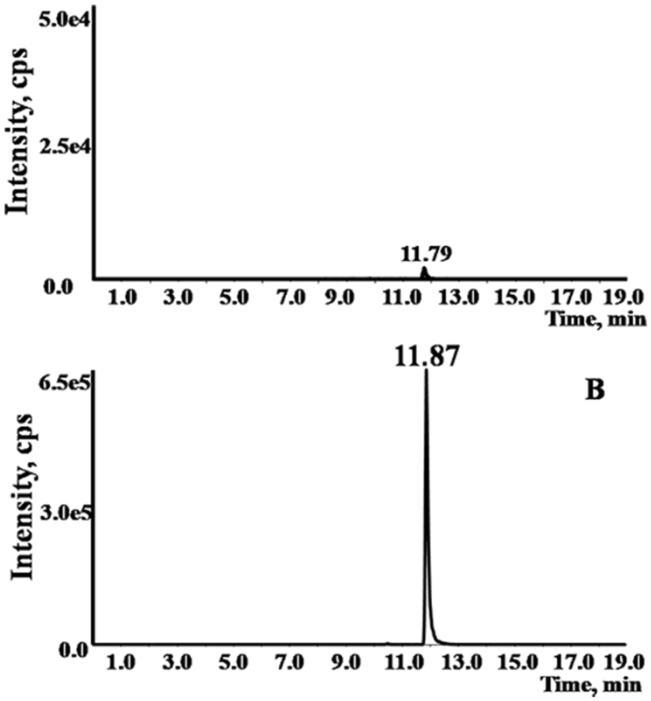

DMD Fast Forward. Published on October 11, 2017 as DOI: 10.1124/dmd.117.077818
This article has not been copyedited and formatted. The final version may differ from this version.

Figure 8.

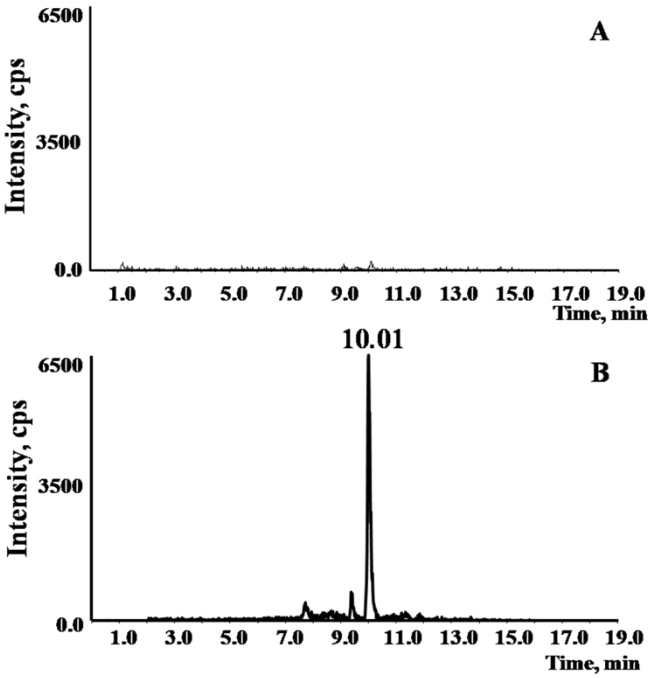

DMD Fast Forward. Published on October 11, 2017 as DOI: 10.1124/dmd.117.077818
This article has not been copyedited and formatted. The final version may differ from this version.

Figure 9.

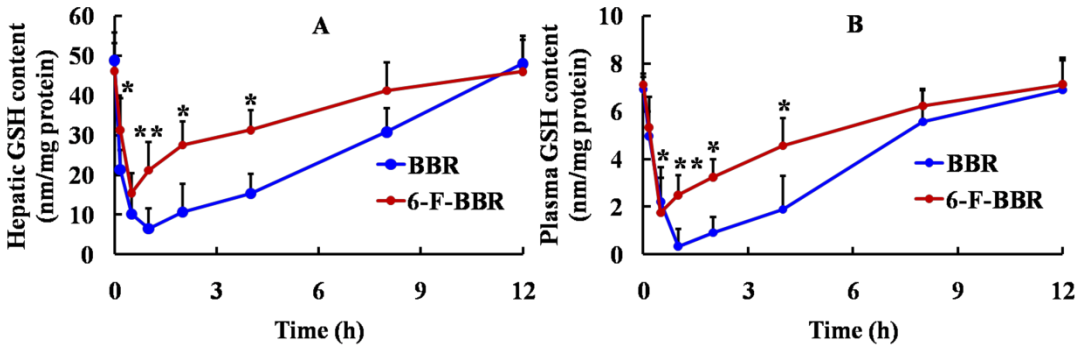

DMD Fast Forward. Published on October 11, 2017 as DOI: 10.1124/dmd.117.077818
This article has not been copyedited and formatted. The final version may differ from this version.

Figure 10.

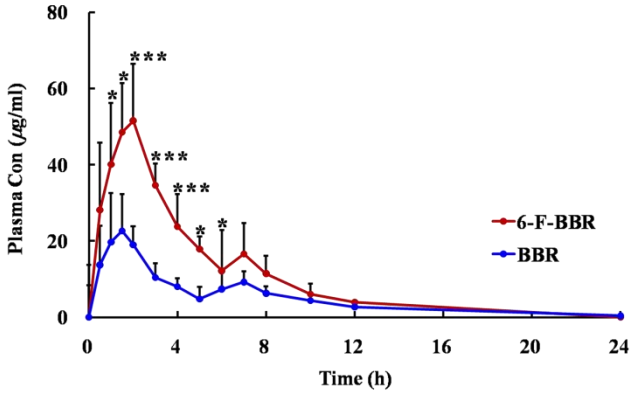

DMD Fast Forward. Published on October 11, 2017 as DOI: 10.1124/dmd.117.077818
This article has not been copyedited and formatted. The final version may differ from this version.

Scheme 1.